



Cite this: *RSC Adv.*, 2025, **15**, 49301

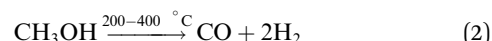
Received 19th September 2025  
 Accepted 1st December 2025

DOI: 10.1039/d5ra07097j  
[rsc.li/rsc-advances](http://rsc.li/rsc-advances)

## Mechanism of methanol steam reforming with inverse $\text{ZrO}_2/\text{Cu}$ catalyst

Jie Feng,<sup>†a</sup> Tingting Zhang,<sup>†c</sup> Guozhi Zhao,<sup>b</sup> Chengxiang Li,<sup>b</sup> Xuan Wu,<sup>b</sup> Jiaqiang Sun,<sup>†b</sup> Yu Wang,<sup>\*,d</sup> Kun Liu<sup>†d</sup> <sup>\*e</sup> and Guofeng Zhao<sup>\*,ab</sup>

The highly active inverse  $\text{ZrO}_2/\text{Cu}$  catalyst used in methanol steam reforming reaction was confirmed by XRD and HRTEM. Control experiments and characterization results consistently differentiated surface and interfacial hydroxyl groups. For the catalyst enriched in interfacial OH, the reaction preferentially proceeded through the formate pathway. However, for the catalyst enriched in surface OH, methyl formate pathway preferentially existed on its surface. This work reveals the role of OH plays in the methanol steam reforming reaction, preliminarily establishing foundation for the investigation of  $\text{H}_2\text{O}$ -participated reactions.



## 1 Introduction

Hydrogen energy, as a clean and renewable energy source, plays a crucial role in resolving the global energy crisis and mitigating environmental challenges. However, its widespread application is currently restrained by issues such as storage safety risks, high transportation costs, and the difficulty of hydrogen production.<sup>1,2</sup> In contrast, methanol, with a high hydrogen content of up to 12.5 wt% and relatively safe transport properties, has emerged as a promising carrier for hydrogen storage and transportation.<sup>3-7</sup> The hydrogen stored in methanol can be efficiently released *via* the methanol steam reforming (MSR) reaction (eqn (1)). Nevertheless, side reaction occurring during the MSR process (eqn (2)) decreases hydrogen impurity, which significantly hinders its practical utilization. Therefore, the development of high efficient MSR catalyst and the comprehensive understanding of the MSR mechanism is of great importance.<sup>1,8,9</sup>



<sup>a</sup>Shanghai Key Laboratory of Green Chemistry and Chemical Processes, School of Chemistry and Molecular Engineering, East China Normal University, Shanghai 200062, China. E-mail: gfzhao@ahnu.edu.cn

<sup>b</sup>Anhui Basic Discipline Research Center for Clean Energy and Catalysis, College of Chemistry and Materials Science, Anhui Normal University, Wuhu 241002, China

<sup>c</sup>School of Foreign Languages, Shandong First Medical University & Shandong Academy of Medical Sciences, Tai'an 271016, China

<sup>d</sup>Frontiers Science Center for Transformative Molecules, Zhangjiang Institute for Advanced Study, Shanghai Jiao Tong University, Shanghai 200240, China. E-mail: wangyusjtu@sjtu.edu.cn

<sup>e</sup>Institute of Optical Functional Materials for Biomedical Imaging, School of Chemistry and Pharmaceutical Engineering, Shandong First Medical University & Shandong Academy of Medical Sciences, Tai'an 271016, China. E-mail: liukun2436@126.com

† The authors contribute equally to this work.

MSR reaction is a complex, multi-step process including the steps such as methanol dehydrogenation, hydroxyl dissociation, and the water-gas shift reaction.<sup>10</sup> The reaction mechanism is commonly proposed to proceed *via* three primary pathways: (1) methanol undergoes dehydrogenation to form formaldehyde, which subsequently decomposes into carbon monoxide and hydrogen; carbon monoxide then reacts with water through the water-gas shift reaction, yielding carbon dioxide and hydrogen.<sup>11</sup> (2) Methanol dehydrogenates to generate methoxy species, which react with methanol to produce methyl formate; methyl formate subsequently decomposes into formate species, which further decompose into carbon dioxide and hydrogen.<sup>12</sup> (3) Methanol dehydrogenates to form formaldehyde, which is oxidized by water to form formic acid; formic acid then decomposes into carbon dioxide and hydrogen.<sup>13</sup> Hence, a comprehensive investigation of the reaction mechanism, particularly the structure-function relationships of active sites, is essential for enhancing the efficiency and selectivity of the reaction.<sup>14</sup> Such insights also provide a scientific basis for the rational design of catalysts, facilitating industrial-scale applications.

In our previous work, we have developed an effective inverse  $\text{ZrO}_2/\text{Cu}$  ( $\text{ZrO}_2$ : ~2–3 nm, Cu: ~10–15 nm) for the MSR reaction.<sup>15</sup> The work mainly investigated the adsorption and desorption of the intermediates such as  $\text{HCHO}$ ,  $\text{HCOOCH}_3$ . Additionally, traditional  $\text{Cu}/\text{ZrO}_2$  or inverse  $\text{ZrO}_2/\text{Cu}$  have also been reported in the MSR reaction by other groups and the effects (such as the pivotal intermediate  $\text{HCOO-Cu}$ ,<sup>16</sup> Cu size,<sup>17</sup> Cu valence,<sup>17</sup> and  $\text{ZrO}_2$  crystal phase<sup>18</sup>) have been investigated. However, the role of hydroxyl species playing in MSR reaction is still unclear. Moreover, the hydroxyl species plays an important



role in  $\text{H}_2\text{O}$ -related reactions, such as MSR reaction,<sup>19</sup> water gas shift reaction,<sup>20</sup> and CO preferential oxidation reactions.<sup>21</sup> This work reveals that on the  $\text{ZrO}_2/\text{Cu}$  catalyst, the surface OH (on  $\text{ZrO}_2$  surface) and interfacial OH (at  $\text{ZrO}_2$ -Cu interface) coexist, the interfacial OH being more active in the MSR reaction. *In situ* diffuse reflectance infrared fourier-transform spectroscopy (*in situ* DRIFTS) confirmed that methanol adsorbed on surfaces rich in interfacial hydroxyl groups undergoes the formate pathway,<sup>22</sup> leading to the formation of  $\text{CO}_2$  and  $\text{H}_2$  ( $\text{CH}_3\text{OH} + \text{interfacial OH} \rightarrow \text{CH}_3\text{O}^*, \text{CH}_3\text{O}^* + \text{interfacial OH} \rightarrow \text{HCOOH} \rightarrow \text{CO}_2 + \text{H}_2\text{O}$ ). In contrast, on surfaces with surface hydroxyl groups, which react with methanol to produce  $^*\text{COOH}$ . Subsequently,  $^*\text{COOH}$  reacts with  $\text{CH}_3\text{OH}$  to form methyl formate. Finally, methyl formate decomposes to  $\text{CH}_3\text{O}^*$  ( $\text{CH}_3\text{O}^*$  transform to formate to accomplish to catalytic cycle) ( $\text{CH}_3\text{OH} + \text{surface OH} \rightarrow ^*\text{COOH}, ^*\text{COOH} + \text{CH}_3\text{OH} \rightarrow \text{HCOOCH}_3 \rightarrow \text{CH}_3\text{O}^*, \text{CH}_3\text{O}^* + \text{minor interfacial OH} \rightarrow \text{HCOOH} \rightarrow \text{CO}_2 + \text{H}_2\text{O}$ ). This reaction mechanism highlights the critical role of hydroxyl groups in determining catalytic performance, establishing the foundation of developing high performance MSR catalysts.

## 2 Experimental

The detailed catalyst preparation, catalyst characterization, and catalyst evaluation (Fig. S1) were exhibited in the SI. Note that: fresh  $\text{ZrO}_2$ -0.25/Cu (weight content of  $\text{ZrO}_2$  was 25%) without other pre-treatment condition, the sample was abbreviated as  $\text{ZrO}_2$ -0.25/Cu-dried. For the fresh  $\text{ZrO}_2$ -0.25/Cu under ( $\text{H}_2\text{O}$ -bubbling atmosphere  $\text{H}_2\text{O}$  bubbling in He flow (30 mL min<sup>-1</sup>) for 30 min), the sample was labelled as  $\text{ZrO}_2$ -0.25/Cu-humidified. For the fresh  $\text{ZrO}_2$ -0.25/Cu after reduced ( $\text{H}_2/\text{He}$  mixed gas (5 vol%  $\text{H}_2$ )) for 30 min, (300 °C), the sample was named as  $\text{ZrO}_2$ -0.25/Cu-reduced.

## 3 Results and discussion

### 3.1 Structures and chemical states of catalysts

In our previous work, we found that  $\text{ZrO}_2$ -0.1/Cu exhibited excellent catalytic performance in MSR reaction (~60% methanol conversion and 100%  $\text{CO}_2$  selectivity at 250 °C).<sup>15</sup> However, for this catalyst, we found that the OH species couldn't be detected by *in situ* DRIFTS. Hence,  $\text{ZrO}_2$ -0.25/Cu (the weight content of  $\text{ZrO}_2$  was 0.25) was selected to investigate the role of OH species playing in this reaction ( $\text{ZrO}_2$ -0.25/Cu exhibited ~60% methanol conversion and 100%  $\text{CO}_2$  selectivity at 250 °C, Fig. S2). XRD pattern (Fig. 1A) revealed that only characteristic diffraction peaks of  $\text{CuO}$  phase were detected, with the most prominent peak intensity observed for the (111) crystal plane. Notably, no characteristic diffraction peaks of  $\text{ZrO}_2$  were identified. Subsequent quantitative analysis of  $\text{ZrO}_2$  loading through ICP-OES (Table S1) demonstrated that  $\text{ZrO}_2$  loading of 22.01 wt% in the  $\text{ZrO}_2$ -0.25/Cu catalyst. This finding aligns with the absence of  $\text{ZrO}_2$  crystalline phase detection in XRD patterns, indicating that  $\text{ZrO}_2$  exists in a highly dispersed state on the  $\text{CuO}$  surface,<sup>23</sup> which is consistent with our previous studies.<sup>15</sup> To investigate the surface morphology of the catalyst,

transmission electron microscopy (TEM) analysis was performed (Fig. 1B). Distinct lattice fringes with spacings of 0.254 nm and 0.294 nm were clearly observed on the  $\text{ZrO}_2$ -0.25/Cu surface, corresponding to the (111) plane of  $\text{CuO}$  and the (011) plane of tetragonal  $\text{ZrO}_2$  ( $t\text{-ZrO}_2$ ), respectively.<sup>24</sup> This observation further confirms the uniform dispersion of fine ~3–4 nm  $t\text{-ZrO}_2$  particles on the ~10–15 nm  $\text{CuO}$  substrate in the  $\text{ZrO}_2$ -0.25/Cu catalyst, rather than the absence of  $t\text{-ZrO}_2$  components.<sup>25</sup> Moreover, for the reduced catalyst, XRD and TEM techniques (Fig. 1A and C) indicated that the  $\text{ZrO}_2/\text{CuO}$  composite transforms to  $\text{ZrO}_2/\text{Cu}$  ( $\text{ZrO}_2$ , 3–4 nm, Cu 15–20 nm;  $\text{ZrO}_2$  and Cu particle size derived from Scherrer equation are 3.5 and 16 nm, respectively), which may play an important role in the MSR reaction. The well-defined lattice structures and interfacial characteristics align with previous reports on  $\text{Cu}/\text{ZrO}_2$  heterojunction systems, where such structural configurations enhance catalytic performance through synergistic effects.

### 3.2 Distinguish surface OH from interfacial OH

Derived from previous works, OH plays an important role in the  $\text{H}_2\text{O}$ -related reactions,<sup>26</sup> but the surface and interfacial OH hasn't been investigated. From these previous works, we know that  $\text{H}_2$ -reduction or  $\text{H}_2\text{O}$  ( $\text{D}_2\text{O}$ )-bubbling are two vital roles to introduce OH (OD) into the catalyst. So,  $\text{ZrO}_2$ -0.25/Cu-dried,  $\text{ZrO}_2$ -0.25/Cu-humidified, and  $\text{ZrO}_2$ -0.25/Cu-reduced were tentatively investigated by  $\text{H}_2\text{O}$ -TPD to investigate the surface and interfacial OH (Fig. 2).  $\text{H}_2\text{O}$ -TPD profiles reveal two characteristic desorption regions: peak at 180–200 °C corresponding to active interfacial hydroxyl groups (at  $\text{ZrO}_2/\text{Cu}$  interface), and those near 340 °C representing weakly active surface hydroxyl species (on  $\text{ZrO}_2$  surface).<sup>27</sup> Notably, the  $\text{ZrO}_2$ -0.25/Cu-dried exhibited a minor concentration of hydroxyl groups, probably contributing to its negligible catalytic activity (~1% methanol conversion at 250 °C). Meanwhile, the  $\text{ZrO}_2$ -0.25/Cu-humidified shows substantially quantities of surface hydroxyl groups, likely corresponding with its inferior catalytic activity (~5% methanol conversion at 250 °C). Remarkably and interestingly, for  $\text{ZrO}_2$ -0.25/Cu-reduced, apart from the surface hydroxyl groups at 340 °C, the prominent  $\text{H}_2\text{O}$ -desorption peak at 180–200 °C appeared, tentatively attributed to interfacial OH and corresponding with its excellent catalytic activity (~60% methanol conversion at 250 °C).

Subsequently,  $\text{CH}_3\text{OH}$ -adsorbed  $\text{ZrO}_2$ -0.25/Cu-dried,  $\text{ZrO}_2$ -0.25/Cu-humidified, and  $\text{ZrO}_2$ -0.25/Cu-reduced at different temperatures were investigated by *in situ* DRIFTS to differentiate surface from interfacial OH (Fig. 3). The absorption bands at 3650–3550 cm<sup>-1</sup> are attributed to isolated hydroxyl groups on the zirconia surface, those at 3700–3650 cm<sup>-1</sup> correspond to surface hydroxyl groups on zirconia,<sup>28</sup> and those at 3750–3700 cm<sup>-1</sup> are associated with interfacial hydroxyl groups between zirconia and copper, predominantly in the form of  $\text{Zr}-(\text{OH})-\text{Cu}$ .<sup>29</sup> For  $\text{ZrO}_2$ -0.25/Cu-dried, the interfacial hydroxyl group content is nearly absent (Fig. 2). At 175 °C, as methanol enters the reaction, the hydroxyl groups undergo transformations. Upon methanol introduction, methanol undergoes decomposition on the zirconia surface, generating methoxy and



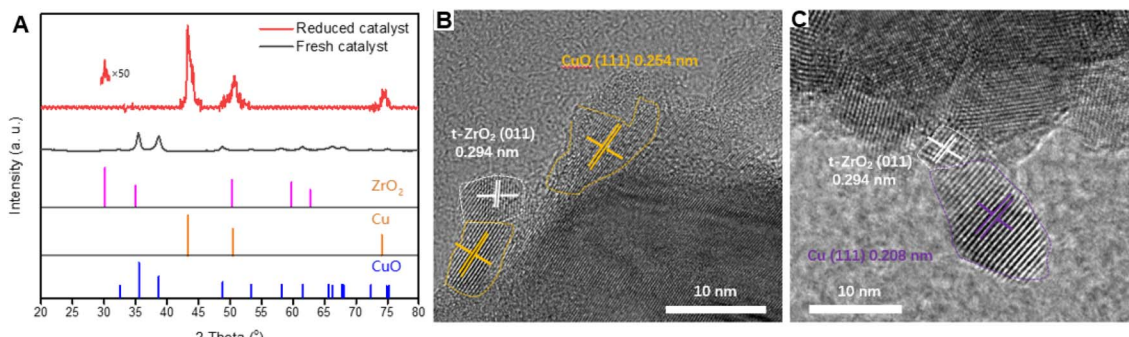


Fig. 1 (A) XRD patterns of fresh ZrO<sub>2</sub>-0.25/Cu and ZrO<sub>2</sub>-0.25/Cu-reduced; (B) HRTEM image of fresh ZrO<sub>2</sub>-0.25/Cu; (C) HRTEM image of ZrO<sub>2</sub>-0.25/Cu-reduced.

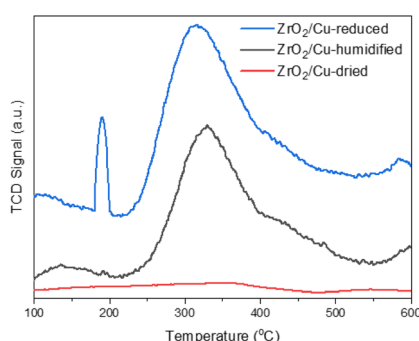


Fig. 2 H<sub>2</sub>O-TPD profiles of ZrO<sub>2</sub>/Cu-reduced, ZrO<sub>2</sub>/Cu-humidified, and ZrO<sub>2</sub>/Cu-dried.

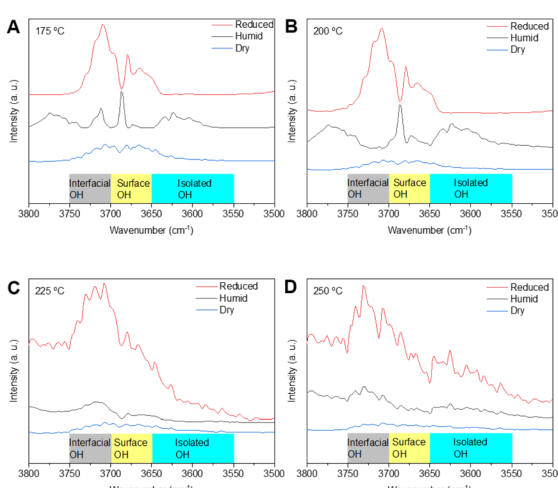


Fig. 3 Amplified *in situ* DRIFTS (3800–3500 cm<sup>-1</sup>, to differentiate surface OH from interfacial OH) of ZrO<sub>2</sub>/Cu-reduced, ZrO<sub>2</sub>/Cu-humidified, and ZrO<sub>2</sub>/Cu-dried after methanol reaction for 3 min at different temperatures ((A) 175 °C, (B) 200 °C, (C) 225 °C, (D) 250 °C).

hydrogen species. The hydrogen (from OH of CH<sub>3</sub>OH) preferentially reacts with surface oxygen to form surface hydroxyl groups (Fig. 3). The minimal amount of carbon dioxide detected (corresponding to the C=O stretching vibration at 2360 cm<sup>-1</sup>) indicates low activity of these surface hydroxyl groups (Fig. 4). In

contrast, for ZrO<sub>2</sub>-0.25/Cu-humidified, due to the presence of water, it exhibits a substantial amount of surface hydroxyl groups with minor interfacial hydroxyl groups (Fig. 3), corresponding with its moderate CO<sub>2</sub> production (Fig. 4). For ZrO<sub>2</sub>-0.25/Cu-reduced, the catalyst surface contains a significant amount of interfacial hydroxyl groups (Fig. 3), leading to an unusually high CO<sub>2</sub> yield (Fig. 4). Notably, with the increasing of temperature (175–250 °C), surface OH transforms to interfacial OH, forming the active Zr-(OH)-Cu structure (can be observed for ZrO<sub>2</sub>-0.25/Cu-humidified and obviously found for ZrO<sub>2</sub>-0.25/Cu-reduced). Hence, the interfacial OH plays an important role in MSR reaction and a part of surface OH could transforms to interfacial OH.

### 3.3 Reaction mechanism

In the MSR reaction, H<sub>2</sub>O can dissociate at the surface or the interface site to form OH species.<sup>30</sup> For ZrO<sub>2</sub>-0.25/Cu-dried, with the increase of temperature from 175 °C to 250 °C, the C=O stretching vibrations of methyl formate (Fig. 5, at 1740 and

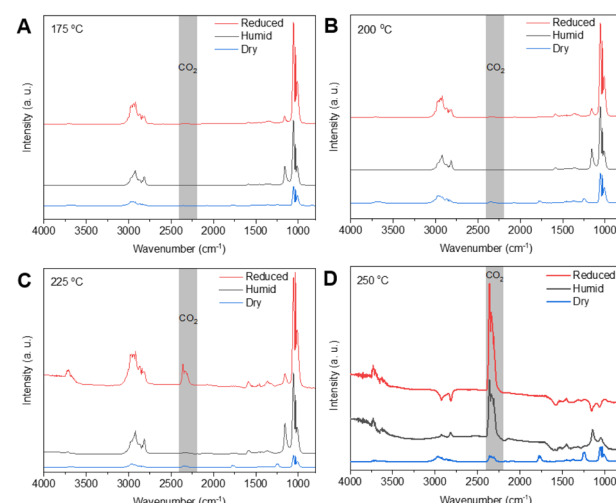


Fig. 4 Amplified *in situ* DRIFTS (4000–900 cm<sup>-1</sup>, to differentiate CO<sub>2</sub>) of ZrO<sub>2</sub>/Cu-reduced, ZrO<sub>2</sub>/Cu-humidified, and ZrO<sub>2</sub>/Cu-dried after methanol reaction for 3 min at different temperatures ((A) 175 °C, (B) 200 °C, (C) 225 °C, (D) 250 °C).

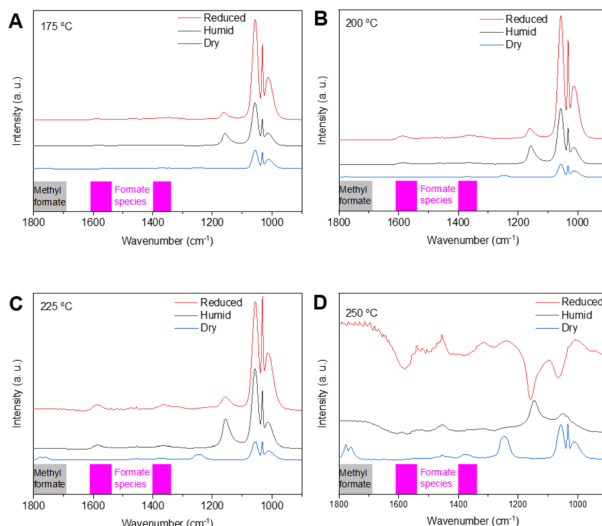


Fig. 5 Amplified *in situ* DRIFTS (1800–900  $\text{cm}^{-1}$ , to differentiate methyl formate from formate species) of  $\text{ZrO}_2/\text{Cu}$ -reduced,  $\text{ZrO}_2/\text{Cu}$ -humidified, and  $\text{ZrO}_2/\text{Cu}$ -dried after methanol reaction for 3 min at different temperatures ((A) 175 °C, (B) 200 °C, (C) 225 °C, (D) 250 °C).

1780  $\text{cm}^{-1}$ ) increase progressively.<sup>23</sup> Meanwhile, no significant change attributed to surface OH is observed in the peak region at 3700–3650  $\text{cm}^{-1}$  (Fig. 3), and the peak at 2360  $\text{cm}^{-1}$  assigned as  $\text{CO}_2$  (Fig. 4) is considerably lower compared to the other two samples. These observations consistently suggest that in the

absence of interfacial hydroxyl groups, the reaction preferentially proceeds *via* the methyl formate pathway (Fig. 6A), resulting in low catalytic activity. For  $\text{ZrO}_2\text{-}0.25/\text{Cu}$ -humidified and  $\text{ZrO}_2\text{-}0.25/\text{Cu}$ -reduced, interfacial hydroxyl groups coexist on the catalyst surface. However,  $\text{ZrO}_2\text{-}0.25/\text{Cu}$ -reduced exhibits a higher interfacial hydroxyl content. With the increase of temperature from 175 to 250 °C, formate species (at 1580 and 1380  $\text{cm}^{-1}$ , corresponding to the asymmetric and symmetric COO) is appeared (Fig. 5), with the intensity of  $\text{ZrO}_2\text{-}0.25/\text{Cu}$ -reduced being higher.<sup>31</sup> Meanwhile,  $\text{CO}_2$  content displays a relatively higher content (Fig. 4). These findings indicate that, in the presence of interfacial hydroxyl groups, the reaction proceeds through the formate pathway (Fig. 6B), leading to significantly enhanced catalytic activity. For  $\text{ZrO}_2\text{-}0.25/\text{Cu}$ -dried, with the increase of temperature from 175 °C to 250 °C, the C=O stretching vibrations of methyl formate (Fig. 5, at 1740 and 1780  $\text{cm}^{-1}$ ) increase progressively.<sup>20</sup> Meanwhile, no significant change attributed to surface OH is observed in the peak region at 3700–3650  $\text{cm}^{-1}$  (Fig. 3), and the peak at 2360  $\text{cm}^{-1}$  assigned as  $\text{CO}_2$  (Fig. 4) is considerably lower compared to the other two samples. These observations consistently suggest that in the absence of interfacial hydroxyl groups, the reaction proceeds *via* the methyl formate pathway (Fig. 6A), resulting in low catalytic activity. For  $\text{ZrO}_2\text{-}0.25/\text{Cu}$ -humidified and  $\text{ZrO}_2\text{-}0.25/\text{Cu}$ -reduced, interfacial hydroxyl groups coexist on the catalyst surface. However,  $\text{ZrO}_2\text{-}0.25/\text{Cu}$ -reduced exhibits a higher interfacial hydroxyl content. With the increase of temperature from 175 to 250 °C, formate species (at 1580 and

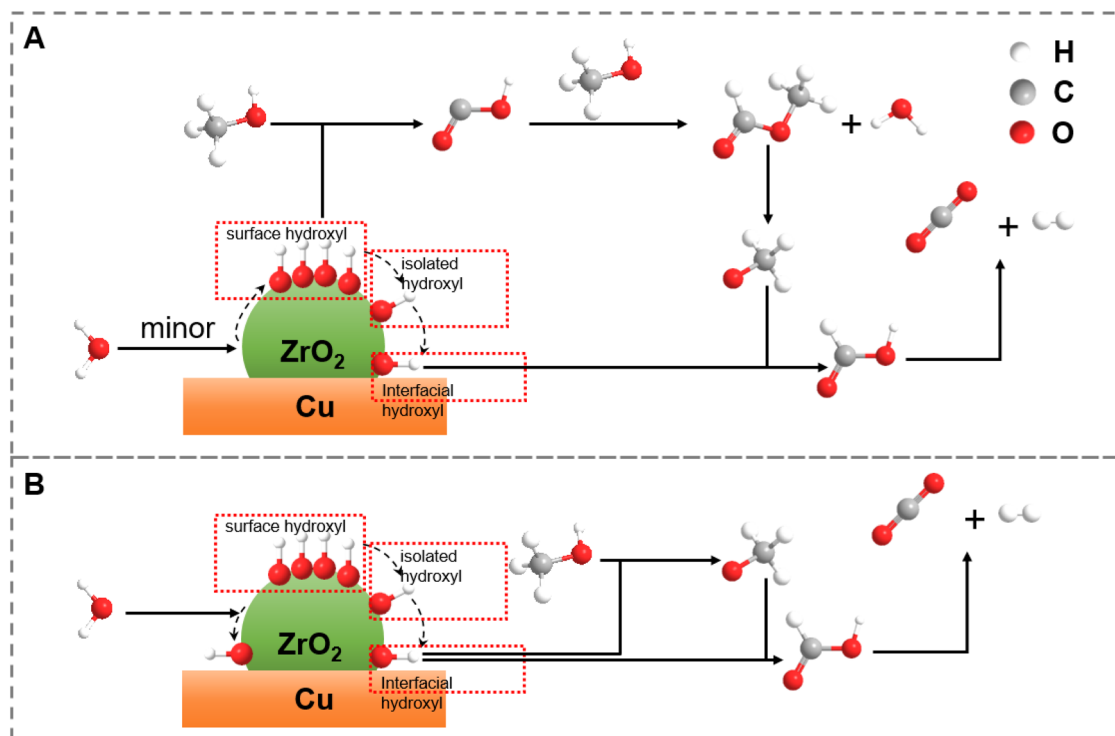


Fig. 6 Reaction mechanism of MSR reaction on  $\text{ZrO}_2/\text{Cu}$ . (A) Catalyzed by surface OH through methyl formate pathway:  $\text{CH}_3\text{OH} + \text{surface OH} \rightarrow *_{\text{COOH}}$ ,  $*_{\text{COOH}} + \text{CH}_3\text{OH} \rightarrow \text{HCOOCH}_3 \rightarrow \text{CH}_3\text{O}^*$ ,  $\text{CH}_3\text{O}^* + \text{minor interfacial OH} \rightarrow \text{HCOOH} \rightarrow \text{CO}_2 + \text{H}_2\text{O}$  (B) catalyzed by interfacial OH via formate species pathway:  $\text{CH}_3\text{OH} + \text{interfacial OH} \rightarrow \text{CH}_3\text{O}^*$ ,  $\text{CH}_3\text{O}^* + \text{interfacial OH} \rightarrow \text{HCOOH} \rightarrow \text{CO}_2 + \text{H}_2\text{O}$ .



1380  $\text{cm}^{-1}$ , corresponding to the asymmetric and symmetric COO is appeared (Fig. 5), with the intensity of  $\text{ZrO}_2\text{-0.25/Cu}$ -reduced being higher.<sup>27</sup> Meanwhile,  $\text{CO}_2$  content displays a relatively higher content (Fig. 4). These findings indicate that, in the presence of interfacial hydroxyl groups, the reaction preferentially proceeds through the formate pathway (Fig. 6B), leading to significantly enhanced catalytic activity.

### 3.4 Discussion

Moreover, in order to further corroborate the pivotal role of interfacial OH playing in MSR reaction, the control experiments were designed. From the  $\text{H}_2\text{O-TPD}$  experiment, we know that the peaks at  $\sim 200$  and  $\sim 300\text{--}400$   $^\circ\text{C}$  are attributed to the removal of interfacial and surface OH (Fig. 2). Hence, we treated the  $\text{ZrO}_2\text{/Cu}$ -reduced under pure He flow at 180  $^\circ\text{C}$  to partly remove the interfacial OH. Form Fig. S4, with the treatment time from 1 to 5 min, the peaks (at  $\sim 200$   $^\circ\text{C}$ ) corresponding to interfacial OH decease suddenly and the ones corresponding to surface OH (at 300  $\text{--}$  400  $^\circ\text{C}$ ) are nearly unchanged. Meanwhile, the He-treated  $\text{ZrO}_2\text{/Cu}$ -reduced (He: 1, 5 min) could also catalyze methanol steam reforming reaction at 180  $^\circ\text{C}$  just using the residual interfacial OH (200 mg catalyst,  $\text{N}_2$  flow of 30  $\text{mL min}^{-1}$ , and methanol of 1  $\text{g h}^{-1}$ ). The initial methanol conversions using the  $\text{ZrO}_2\text{/Cu}$ -reduced,  $\text{ZrO}_2\text{/Cu}$ -reduced-He-1 min ( $\text{ZrO}_2\text{/Cu}$ -reduced treated under He flow for 1 min at 180  $^\circ\text{C}$ ), and  $\text{ZrO}_2\text{/Cu}$ -reduced-He-5 min ( $\text{ZrO}_2\text{/Cu}$ -reduced treated under He flow for 5 min at 180  $^\circ\text{C}$ ) catalyst were 7%, 2%, 1%, respectively, corresponding well with the  $\text{H}_2\text{O-TPD}$  spectra. Hence, the control experiment further testifies the pivotal role of interfacial OH other than surface OH playing in this reaction.

Up to date, most endeavors are focused on Cu-based catalysts, especially  $\text{Cu-ZrO}_2$ , because of their attractive low-temperature MSR activity and its substantial potential against CO formation.<sup>15</sup> For example, Ritzkopf *et al.*<sup>32</sup> prepared a nano- $\text{Cu/ZrO}_2$  catalyst by the micro-emulsion method, achieving a lower CO selectivity of below 0.1 vol% at 300  $^\circ\text{C}$  with a hydrogen productivity comparable to the commercial  $\text{Cu/ZnO}$  catalyst. Indeed, in the whole process, for our inverse  $\text{ZrO}_2\text{/Cu}$  and  $\text{Cu/ZrO}_2$ ,<sup>32</sup> catalysts, the CO selectivity is very low. Thus, we confidently believe that the  $\text{Cu-ZrO}_2$  interface is beneficial to the formation of  $\text{CO}_2$  other than CO (both inverse  $\text{ZrO}_2\text{/Cu}$  and traditional  $\text{Cu/ZrO}_2$  interface) at low temperature ( $<300$   $^\circ\text{C}$ ). From the  $\text{H}_2\text{O-TPD}$  results (Fig. S5), we could see that for the traditional  $\text{Cu/ZrO}_2$ ,<sup>32</sup> the content of interfacial OH is similar to that of our inverse  $\text{ZrO}_2\text{/Cu}$ , so, our inverse  $\text{ZrO}_2\text{/Cu}$  exhibits similar activity (250  $^\circ\text{C}$ , 60% methanol conversion and 99.9%  $\text{CO}_2$  selectivity) compared with that of traditional  $\text{Cu/ZrO}_2$  (250  $^\circ\text{C}$ , 58% methanol conversion and 99.9%  $\text{CO}_2$  selectivity<sup>32</sup>).

## 4 Conclusion

Through  $\text{H}_2\text{O-TPD}$  and *in situ* DRIFTS analyses, we identified that MSR reaction preferentially proceeds through the formate pathway on the highly active  $\text{ZrO}_2\text{-0.25/Cu}$ -reduced catalyst enriched with interfacial hydroxyl groups. However, for  $\text{ZrO}_2\text{-0.25/Cu}$ -dried, methyl formate pathway preferentially exists on

its surface, due to the existence of surface hydroxyl groups (absence of interfacial hydroxyl groups). These findings provide a novel perspective for the design of metal-oxide model catalysts, offering valuable insights to accelerate the industrial application of such systems.

## Conflicts of interest

The authors declare that there is no conflicts of interest.

## Data availability

The data that support the findings of this study are available on request from the corresponding author. The data are not publicly available due to privacy or ethical restrictions.

Supplementary information (SI): the details of catalyst preparation, catalyst characterization, catalyst evaluation, IR flowchart, and  $\text{H}_2\text{O-TPD}$ . See DOI: <https://doi.org/10.1039/d5ra07097j>.

## Acknowledgements

This work was funded by the National Natural Science Foundation of China (grant no. 22179038), the high score discipline construction project of Anhui Province (project no. 061920), and the Young People Fund of Shandong first medical university (202201-037).

## References

- 1 M. Xiao, Y. Zhang, X. Wang and L. Liu, *Angew. Chem., Int. Ed.*, 2024, **63**, e202407640.
- 2 M. Zabilskiy, X. Huang, J. Zheng and K. M. Neyman, *Angew. Chem., Int. Ed.*, 2021, **60**, 4912–4920.
- 3 K. Yu, W. Tong and S. Tsang, *Nat. Commun.*, 2012, **3**, 1230.
- 4 L. Lin, W. Zhou and D. Ma, *Nature*, 2017, **544**, 80–83.
- 5 C. Rameshan, W. Stadlmayr and C. B. Klötzer, *Angew. Chem., Int. Ed.*, 2010, **49**, 3224–3227.
- 6 X. He, Y. Wang and H. Liu, *ACS Catal.*, 2019, **9**, 2213–2221.
- 7 J. Shen and C. Song, *Catal. Today*, 2002, **77**, 89–98.
- 8 M. Kusche, A. Friedrich, T. Braun and J. J. Weigand, *Angew. Chem., Int. Ed.*, 2013, **52**, 5022–5025.
- 9 F. Ji, Y. Li, C. Zhou and W. Wang, *Energy Sci. Eng.*, 2019, **7**, 1200–1208.
- 10 A. Hassan, *Int. J. Hydrogen Energy*, 2024, **93**, 1487–1501.
- 11 M. A. Achomo, P. Muthukumar and N. R. Peela, *Int. J. Hydrogen Energy*, 2025, **140**, 1111–1125.
- 12 J. L. C. Fajín, M. Natália and D. S. Cordeiro, *ACS Catal.*, 2022, **12**, 512–526.
- 13 K. Ma, Y. Tian and Z. Zhao, *Chem. Sci.*, 2019, **10**, 2578–2584.
- 14 X. Zhang, M. Zhang and Y. Deng, *Nature*, 2021, **589**, 396–401.
- 15 X. Xu, T. Lan and G. Zhao, *Appl. Catal., B*, 2023, **334**, 122839–122851.
- 16 C. Wu, L. Lin, J. Liu, J. Zhang, F. Zhang, T. Zhou, N. Rui, S. Yao, Y. Deng, F. Yang, W. Xu, J. Luo, Y. Zhao, B. Yan, X. Wen, J. Rodriguez and D. Ma, *Nat. Commun.*, 2020, **11**, 5767.



17 M. Song, W. Zeng, L. Li, X. Wu, G. Li and C. Hu, *Ind. Eng. Chem. Res.*, 2023, **62**, 3898–3908.

18 M. Song, L. Li, X. Wu, H. Cai, G. Li and C. Hu, *Catalysts*, 2024, **14**, 480.

19 R. Thattarathody and M. Artoul, *Ind. Eng. Chem. Res.*, 2018, **57**, 3175–3186.

20 X. Sun, J. Yu and Y. Han, *Nat. Chem.*, 2024, **16**, 2044–2053.

21 I. Sadykov, D. Palagin and F. Krumeich, *J. Catal.*, 2024, **429**, 115363–115374.

22 P. Luo, P. Shi and C. Li, *Appl. Catal., A*, 2025, **689**, 120006–120025.

23 H. Zhao, R. Yu and S. Ma, *Nat. Catal.*, 2022, **5**, 818–831.

24 X. Chen, Z. Feng and D. Zhao, *Catal. Sci. Technol.*, 2022, **12**, 7048–7056.

25 X. Li, Q. Liu and H. Wu, *Chem.*, 2022, **8**, 2148–2162.

26 L. Luo, J. Luo and H. Li, *ACS Catal.*, 2022, **12**, 11272–11280.

27 Y. Hu, Z. Liang and Y. Zhang, *EES Catal.*, 2024, **2**, 365–378.

28 V. F. Kispersky, Y. Chen and S. P. Crossley, *J. Phys. Chem. C*, 2014, **118**, 16424–16433.

29 H. D. Zhu, S. Wang and S. Wang, *Int. J. Hydrogen Energy*, 2025, **109**, 1452–1460.

30 D. Li, R. Qiu, B. Moskowitz, Z. Jiang, H. Gu, Q. Wen, I. Wachs and M. Zhu, *J. Am. Chem. Soc.*, 2025, **147**, 24040–24049.

31 C. Wu, L. Lin and J. Liu, *Nat. Commun.*, 2020, **11**, 5767–5776.

32 I. Ritzkopf, S. Vukojevic, C. Weidenthaler, J. Grunwaldt and F. Schuth, *Appl. Catal., A*, 2006, **302**, 215–223.

